On chip tunable micro ring resonator actuated by electrowetting

Romi Shamai and Uriel Levy*

Department of Applied Physics, The Benin School of Engineering and Computer Science, The Hebrew University of Jerusalem, Jerusalem, 91904, Israel
**Corresponding author: ulevy@cc.huji.ac.il*

Abstract: We demonstrate a tunable on chip polymer waveguide micro ring resonator (MRR) device. The transmission spectrum and extinction ratio are controlled by electrowetting on dielectric (EWOD), via the application of voltage to a droplet. As a result the droplet covers a portion of the MRR waveguide and changes its effective refractive index. This method can be used for efficiently tuning a variety of on chip optical devices, as it offers high index contrast, electrical control and low power consumption.

OCIS codes: (230.5750) Resonators; (230.7408) Wavelength filtering devices; (230.7380) Waveguides, channeled; (230.3990) Micro-optical devices; (999.9999) Optofluidics.

References and links

1. U. Levy and R. Shamai, "Tunable optofluidic devices," Microfluid Nanofluid **4**, 97-105 (2007).
2. N. Chronis, G. L. Liu, K.H. Jeong, L. P. Lee "Tunable liquid-filled microlens array integrated with microfluidic network," Opt. Express **11**, 2370-2378 (2003).
3. L. Pang, U. Levy, K. Campbell, A. Groisman, Y. Fainman, "A set of two orthogonal adaptive cylindrical lenses in a monolith elastomer device," Opt. Express **13**, 9003-9013 (2005).
4. K. Campbell, U. Levy, Y. Fainman, A. Groisman, "Pressure-driven devices with lithographically fabricated composite epoxy-elastomer membranes," Appl. Phys. Lett. **89**, 154105-154107 (2006).
5. K. Campbell, A. Groisman, U. Levy, L. Pang, S. Mookherjea, D. Psaltis, Y. Fainman, "A microfluidic 2x2 optical switch," Appl. Phys. Lett. **85**, 6119-6121 (2004).
6. U. Levy, K. Campbell, A. Groisman, S. Mookherjea, Y. Fainman, "On-chip microfluidic tuning of an optical microring resonator," Appl. Phys. Lett. **88**, 111107-111109 (2006).
7. J. C. Galas, J. Torres, M. Belotti, Q. Kou, Y. Chen, "Microfluidic tunable dye laser with integrated mixer and ring resonator," Appl. Phys. Lett. **86**, 264101-264103 (2005).
8. Z. Li, Z. Zhang, A. Scherer, D. Psaltis, "Mechanically tunable optofluidic distributed feedback dye laser," Opt. Express **14**, 10494-10499 (2006).
9. M. Gersborg-Hansen and A. Kristensen, "Tunability of optofluidic distributed feedback dye lasers," Opt. Express **15**, 137-142 (2007).
10. D. Erickson, T. Rockwood, T. Emery, A. Scherer, D. Psaltis, "Nanofluidic tuning of photonic crystal circuits," Opt. Lett. **31**, 59-61 (2006).
11. D. B.Wolfe, R. S. Conroy, P. Garstecki, B. T. Mayers, M. A, Fischbach, K. E. Paul, M. Prentiss, G. M. Whitesides, "Dynamic control of liquid-core/liquid-cladding optical waveguides," PNAS **101**, 12434-12438 (2004).
12. F. Mugele and J-C Baret, "Electrowetting: from basics to applications," J. Phys. Condens. Matter **17**, R705-R774 (2005).
13. B. Berge and J. Peseux, "Variable focal lens controlled by an external voltage: an application of electrowetting," Eur. Phys. J. E **3**, 159-163 (2000).
14. S. Kuiper and B. H. W. Hendriks, "Variable-focus liquid lens for miniature cameras," Appl. Phys. Lett. **85**, 1128-1130 (2004).
15. R. A. Hayes and B. J. Feenstra, "Video-speed electronic paper based on electrowetting," Nature **425**, 383-385 (2003).
16. N. R. Smith, D. C. Abeysinghe, J. W. Haus, J. Heikenfeld, "Agile wide-angle beam steering with electrowetting microprisms," Opt. Express **14**, 6557-6563 (2006).
17. P. Mach, T. Krupenkin, S. Yang, J. A. Rogers, "Dynamic tuning of optical waveguides with electrowetting pumps and recirculating fluid channels," Appl. Phys. Lett. **81**, 202-204 (2002).

#104407 - $15.00 USD Received 21 Nov 2008; revised 22 Dec 2008; accepted 22 Dec 2008; published 15 Jan 2009

18. S. Berry, J. Kedzierski, B. Abedian, "Low voltage electrowetting using thin fluoroploymer films," J. Colloid Interface Sci. **303**, 517-524 (2006).
19. K.W. Oh, A. Han, S. Bhansali, "A low-temperature bonding technique using spin-on fluorocarbon polymers to assemble Microsystems," J. Micromech. Microeng. **12**, 187–191 (2002).

1. Introduction

Tunable optofluidic devices (TODs [1]) gain their tunability by modifying the geometry or the refractive index of a fluid interacting with light. The application of external pressure is a common method to control TODs, either by allowing an exchange of liquids having different index of refraction, or by applying a gas pressure that assists in modifying the TOD's geometry. Variety of pressure actuated TODs have been demonstrated both in free-space configuration, e.g. lenses [2, 3], diffraction gratings [4] and switches [5], as well as in integrated on chip configuration, e.g. micro ring resonator (MRR) [6], dye lasers [7-9], photonic band gap crystals [10] and waveguides [11]. In addition to pressure actuation, tunability can also be achieved by using electrowetting on dielectric (EWOD) [12]. EWOD is an attractive control mechanism, as it allows controlling the device by using an electrical signal. Common features of EWOD are low power consumption and response time in the millisecond regime. Currently, most of the EWOD driven TODs operate in free space configuration, with demonstrations of liquid lenses [13, 14], displays [15] and prisms [16], although tunable optical fibers have been also demonstrated [17].

In this work we describe the design, fabrication and experimental characterization of an on chip polymer-waveguide MRR utilizing EWOD for the tuning of its optical properties. As shown in Fig. 1, tunability is achieved by controlling the wetting angle of a droplet that is partially covering the MRR. By applying a voltage to the droplet, its wetting angle is modified, and the droplet covers larger area of the MRR. This result in tunability of the effective refractive index of the MRR waveguide, thus the resonant wavelength and the transmission through the device can be modified. In addition, coupling coefficient can also be tuned with the same method by the application of voltage to a droplet inserted from the inlet on the opposite side. This way, the refractive index of the cladding in the vicinity of the coupling region between the bus waveguide and the MRR is modified, offering a different type of modulation of the transmission spectrum based on the tunability of the extinction ratio of the device.

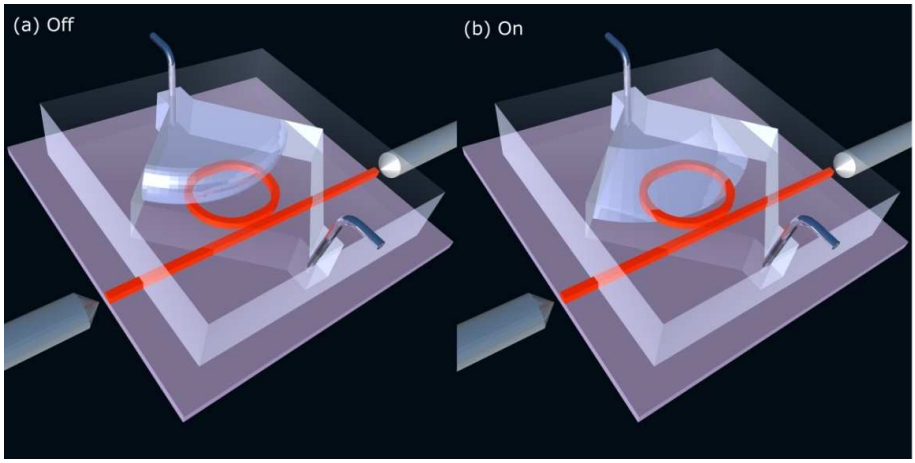

Fig. 1. A schematic model of the EWOD-actuated tunable micro ring resonator. (a) Off state; No voltage is applied and the contact angle between the droplet and the hydrophobic surfaces is high. (b) On state; Voltage is applied, the contact angle is decreased and the droplet covers a larger portion of the MRRs circumference, thus changing the transmission spectrum.

#104407 - $15.00 USD Received 21 Nov 2008; revised 22 Dec 2008; accepted 22 Dec 2008; published 15 Jan 2009

2. Design and fabrication

Fabrication of the device begins with photolithography to define the SU8 waveguides on top of a 2μm thermally grown silica on a highly doped silicon wafer that is used as a surface bottom electrode. We chose the doped silicone electrode rather than a metal electrode because it enables to grow the thermal silicon dioxide layer to form a high quality dielectric insulator. We fabricated two devices, with radii of 200 um and 100 um and a race track length (extended strait length of WG at the coupling region) of 200 um. The WG cross section dimensions are 2μm*2μm. Coupling distance between the bus WG and the ring is designed to be 1 μm. In parallel, a microfluidic chamber of 1.5*1.5*0.4 mm in dimensions, and microfluidic channels connected to this chamber are defined in PDMS by soft lithography. The PDMS is bonded to the silicon chip by applying pressure where Cytop amorphous fluoropolymer is spun on both sides (9% concentration by weight to form a 1 μm thick layer on PDMS and ~2% concentration by weight to form a 100 nm thick layer on silicon dioxide substrate [18]) and used as a bonding material [19]. The effect of the Cytop on the optical properties of the device is negligible, because of its low refractive index (~1.34) and its low thickness. Because of the ratio between the thickness of the oxide and the Cytop layers (~20) and the ratio between their dielectric constants (1.85), the total capacitance due to the Cytop layer is smaller by ~10% compare with the capacitance of the oxide layer. The PDMS and the silicon substrate are pressed together at 120˚C for one hour. In addition to being a good bonding material, Cytop also serves as a hydrophobic layer to increase the wetting angle of the droplet in the off (zero voltage) state as used in many EWOD systems. The thickness of the dielectric insulating layer was chosen to be 2μm as a compromise between two contradictory considerations: 1 – It should be large enough to avoid leakage of optical radiation into the silicon substrate and 2 – it should be thin to reduce the voltage required for electrowetting. Figure 2 shows a schematic cross section of the fabricated device.

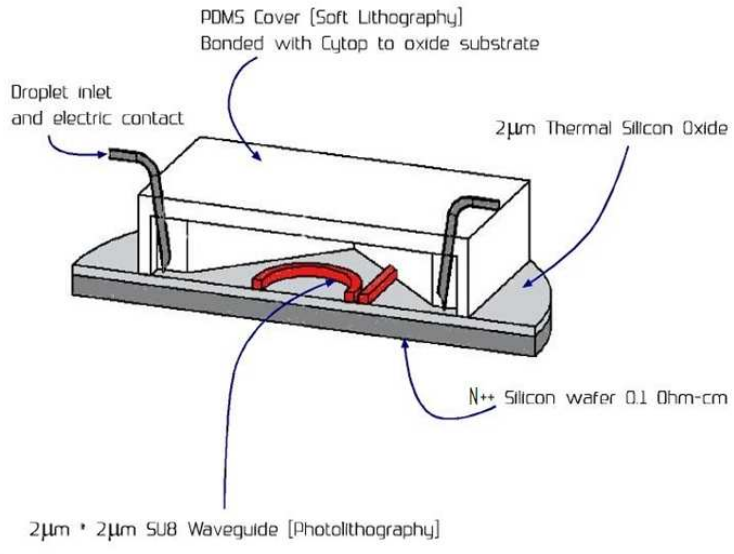

Fig. 2. Schematic cross section of the EWOD-actuated tunable MRR.

#104407 - $15.00 USD Received 21 Nov 2008; revised 22 Dec 2008; accepted 22 Dec 2008; published 15 Jan 2009

3. Device operation and characterization

To operate the fabricated device, a microliter syringe is used to inject a droplet through one of the inlets, towards the vicinity of the MRR that is positioned within the chamber and is about to be tuned. The syringe was filled with a 0.01M solution of Na_2SO_4 in water. Two different configurations are considered: (a) tuning on the ring circumference and (b) tuning on the coupling region.

A TE (in plane) polarized light is coupled from a tunable laser (Agilent 81680A) to the input facet of the bus waveguide using a polarization maintaining tapered fiber with a mode size of 2.5 μm, in a butt coupling configuration. An identical tapered fiber is used to collect light from the output facet of the waveguide. Light is detected by an InGaAs photodetector (HP 81634A).

We first demonstrate modulation of the 200um radius ring. Figure 3 shows the transmission spectrum in the off state (zero voltage) and the on state (285Vrms 1 kHz sinusoidal AC voltage). In the off state, the front end of the droplet is located ~20 μm away from the MRR. In the on state, the wetting angle is reduced and the droplet comes into contact with a ~330 μm length section of the MRR's circumference from the outer side. By observing Fig. 3 one can notice that the droplet is actually stopped at the MRR interface. We believe that this is because the 2 μm thick MRR serves as a physical barrier, preventing the droplet from propagating further into the MRR. The application of voltage results a redshift of about 0.5 nm in the transmission spectrum, resulting a 19 dB modulation in light transmission at wavelength of ~1548 nm.

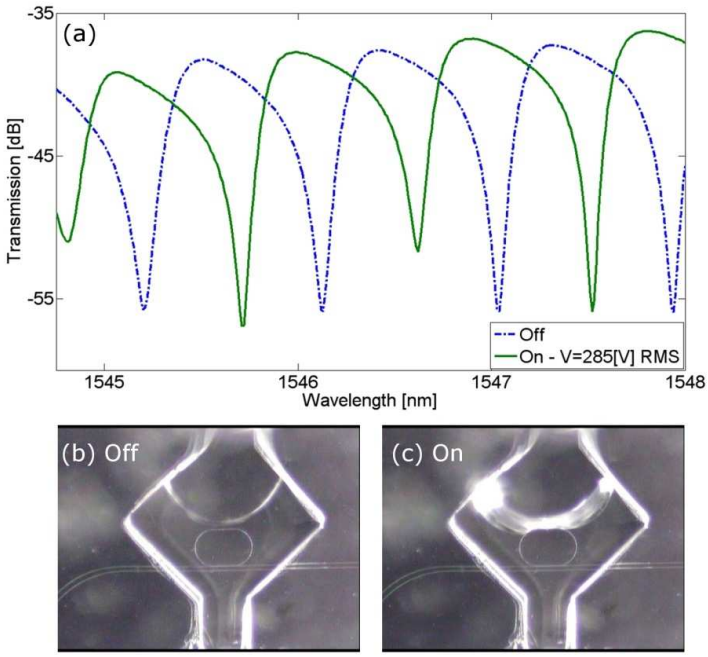

Fig. 3. (a) Transmission spectrum of the MRR in the off (dashed blue curve) and the on (solid green curve) states, where the change occurs mainly over the ring circumference. (b, c) microscope images showing the MRR and the droplet in the off and the on states respectively. Animated presentation of these images: Media 1.

#104407 - $15.00 USD Received 21 Nov 2008; revised 22 Dec 2008; accepted 22 Dec 2008; published 15 Jan 2009

The obtained redshift of 0.5 nm agrees with our theoretical prediction calculated as:

$$\Delta\lambda = \lambda \frac{\Delta n_{eff} \cdot \gamma}{n_{eff}} = 1550 \frac{0.005 \cdot 0.09963}{1.5} = 0.515\,nm \quad (1)$$

where λ is the wavelength (1550 nm), n_{eff} is the effective refractive index of the MRR waveguide (1.5), Δn_{eff} is the change in effective refractive index of the waveguide resulted by changing the medium of the upper cladding from air to water. This value was found to be 0.005 by using the beam propagation method. γ is the relative surface area of the resonator over which the modulation is taking place:

$$\gamma = \frac{A_{cross} \cdot L_{water}}{L_{total}} = \frac{0.5 \cdot 330}{1656} = 0.09963 \quad (2)$$

Where A_{cross} represents the relative amount of WG cross section that is covered by the droplet (we estimate A_{cross} to be about 0.5 in our experiment), L_{water} is the circumference length that is in contact with water (330 μm) and L_{total} is the overall length of the rings circumference (1656 μm).

Next we inject the droplet from the inlet at the opposite side of the ring, to modulate the cladding in the area of the coupling region between the bus waveguide and the MRR. Figure 4 shows the transmission spectrum in the off and the on states. By observing the resonance around 1557 nm wavelength, we notice a drop in extinction ratio from ~25 dB to about 12 dB. Similar trend is noticeable also for the other resonant deeps. To verify the repeatability of operation, we turned off the voltage and measured the spectrum once more. The post wetting results are almost identical to the pre-wetting results.

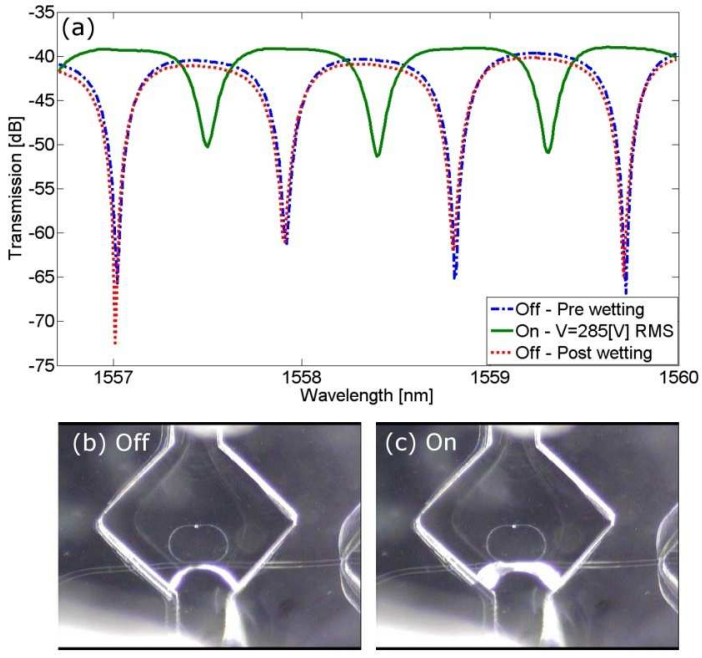

Fig. 4. (a) Transmission spectrum of the MRR in the off (blue dashed and red dotted) and the on (solid green) states, where the modulation occurs over the coupling region. (b, c) microscope images showing the MRR and the droplet in the off and the on states respectively. Animated presentation of these images: Media 2.

#104407 - $15.00 USD Received 21 Nov 2008; revised 22 Dec 2008; accepted 22 Dec 2008; published 15 Jan 2009

The drastic change in extinction ratio is due to the significant change in the coupling coefficient between the bus waveguide and the MRR. As a result, the mismatch between internal loss in the MRR and transmission coefficient increases, leading to a reduction in modulation depth, as expected from the transmission function (Eq. (3)):

$$T = \frac{\alpha^2 + |t|^2 - 2\alpha|t|\cos\theta}{1 + \alpha^2|t|^2 - 2\alpha|t|\cos\theta} \tag{3}$$

where α is the amplitude loss coefficient per round trip (α=1 for a lossless MRR), t is the through coupling coefficient and θ is the phase shift per round trip.

The transmission of the MRR is minimum at resonance, $\theta = 2\pi N$. The transmission at resonance approaches zero at critical coupling, when the values of α and t are closely matched. Therefore, the extinction ratio can be controlled by changing either t or α (or both). To estimate the matching between α and t in the off and the on state we fit left resonance deep shown in Fig. 4 to Eq. (3). We found the values of α and t in the off state (post wetting) to be closely matched with values of 0.590 and 0.576, respectively. On the other hand, by fitting the on state we found values of 0.5629, and 0.7104 for α and t respectively. At a first glance, the increase in t is counter intuitive, because higher refractive index of the upper cladding is expected to increase cross coupling (resulting a decrease in t). However, by carefully observing Fig. 4c we notice that the droplet is in contact only with the outer boundary of the bus waveguide. As a result, the waveguide mode is pulled away from the microring, resulting a lower cross coupling and a higher value of t. This partial coverage of the WG cross section is also in agreement with the value of A_{cross} that was used to calculate the expected redshift in Fig. 3.

In addition to the significant change in modulation depth, a redshift in resonant wavelength of about 0.5 nm is noticeable. This is again due to the increase in the effective refractive index resulting an increase in optical path length in the MRR. Independent control over the resonant wavelength and the modulation depth is feasible via the realization of two droplets, one tuning the coupling region and the other tuning the ring circumference. For example, for the goal of controlling the modulation depth without experiencing a shift in resonance frequency, one can use the two droplets operating in a compensation mode, where the droplet tuning the ring circumference is operated in a reverse mode, i.e. the voltage applied to this droplet should be reduced with the increase of voltage applied to the droplet modulating the coupling region. We intend to demonstrate this concept in the future.

In a second device, with a ring radius of 100 μm, we measured the transmission vs. voltage at a fixed wavelength around 1550 nm. The droplet was set to cover a partial area of the MRR's circumference similarly to the configuration shown in Fig. 1. Here we tuned the laser wavelength to fall within one of the resonances of the MRR, with transmission close to zero. Then we raised the peak to peak amplitude in steps of 50 Volts up to 300 volts (212 RMS). Figure 5 shows the measured transmission (solid blue). To explain the obtained results, we also plot a theoretical curve (dashed red), calculated by a model that is explained below.

#104407 - $15.00 USD Received 21 Nov 2008; revised 22 Dec 2008; accepted 22 Dec 2008; published 15 Jan 2009

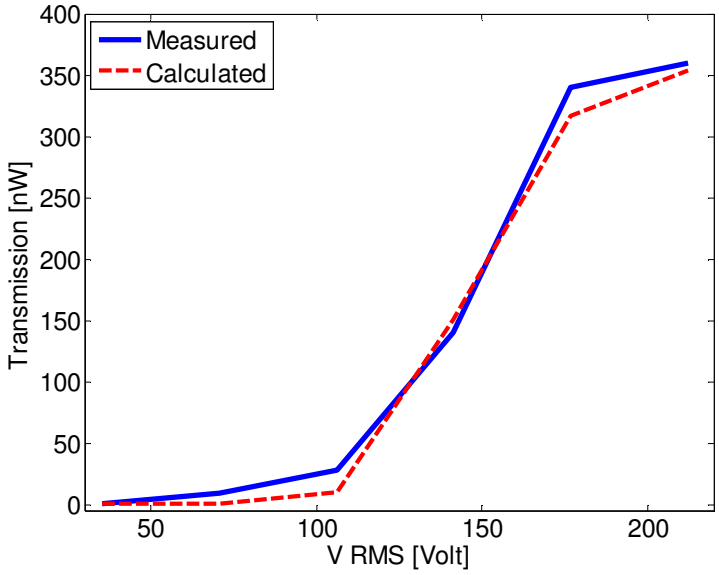

Fig. 5. Measured (solid blue curve) and calculated (dashed red curve) transmission versus voltage, starting at a resonant wavelength with the MRR partially covered by a droplet. As voltage increases the droplet spreads and covers larger portion of the ring's circumference, resulting a shift in the MRR resonant wavelength and an increase in light transmission.

Our model includes the following steps: (a) measuring droplet angle vs. voltage and finding a fit to Young Lippmann equation (Eq. (4)) based on the measured values.

$$\cos\theta = \cos\theta_0 + \frac{1}{2}\frac{C}{\gamma}V^2 \tag{4}$$

From the fitting we obtained $\frac{1}{2}\frac{C}{\gamma} = 2.337 \cdot 10^{-5}\ V^{-2}$, where C is the surface capacitance and γ is the surface tension of the droplet in air. This result is lower by a factor of 4.69 than the theoretical value of this coefficient calculated from known values of water surface tension in air and permittivity of silicon dioxide and Cytop. Detailed study of the reasons for this deviation is beyond the scope of this manuscript, and will be addressed in future work. The measured curve of contact angle dependence on voltage was used to calculate contact angle due to applied voltage in the experiment. (b) Calculated contact angles were used to find the droplet's front line, with the constraints of constant droplet height (resulted by the chamber) droplet circular cross section and constant volume. Droplet frontline at each actuation voltage is shown in Fig. 6.

#104407 - $15.00 USD Received 21 Nov 2008; revised 22 Dec 2008; accepted 22 Dec 2008; published 15 Jan 2009

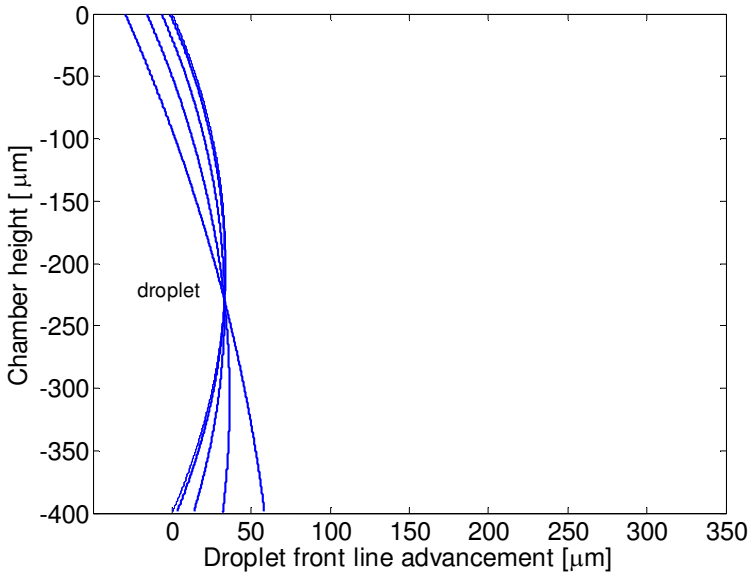

Fig. 6. Calculated cross sections of the droplet inside the chamber at each actuation voltage. The top contact angle is constant at 109.2˚ and the bottom contact angle changes with voltage from 109.2˚ down to 84.4˚. A total advancement of 58.3 μm in the droplet frontline can be seen. The calculation uses the constraints of the chamber height, constant volume of the droplet (constant surface in this 2D cross section), and circular cross section shape of the droplet.

(c) From droplet front line positions and ring geometry we found the lengths of WG that is covered with water as a function of the applied voltage and thus the redshift in resonant wavelengths, according to Eq. (1). (d) By using the redshift values and a typical MRR transmission function (the parameters of the MRR transmission function were chosen to obtain good fit of the model to the experimental results in Fig. 5) we calculated the transmission values. As can be noticed, the transmission curve is not linear. While Eq. (3) implies a nonlinear relation between transmission and voltage, the nearly flat transmission obtained for voltages values up to 100 volts is surprising. Our suggested explanation is that the droplet is pinned on the ring till a certain threshold voltage is reached. To model this we introduced a threshold voltage such that the effective EWOD voltage is the applied voltage minus the threshold voltage. This threshold characteristic is in agreement with the transmission results as shown in Fig. 5.

Due to high sensitivity of the optical response to the droplet position, and difficulties in keeping the position of the droplet fixed over a long period of time we could not perform a detailed characterization of the temporal transfer function of the device, because it requires repeating the experiment with identical conditions for different frequencies of operation. Yet, we estimate the time response of the device by modulating the sinusoidal AC signal of 1 kHz to give a single sinusoidal period every 100 periods (resulting in frequency of 10 Hz). The output optical signal was detected by a photodetector (New Focus 2011-FC), with response time of 2 μsec, that was connected to an Oscilloscope. The measured rise time is about 200 μsec and fall time is about 700 μsec. Improving time response of such devices could be achieved by using smaller droplets.

#104407 - $15.00 USD Received 21 Nov 2008; revised 22 Dec 2008; accepted 22 Dec 2008; published 15 Jan 2009

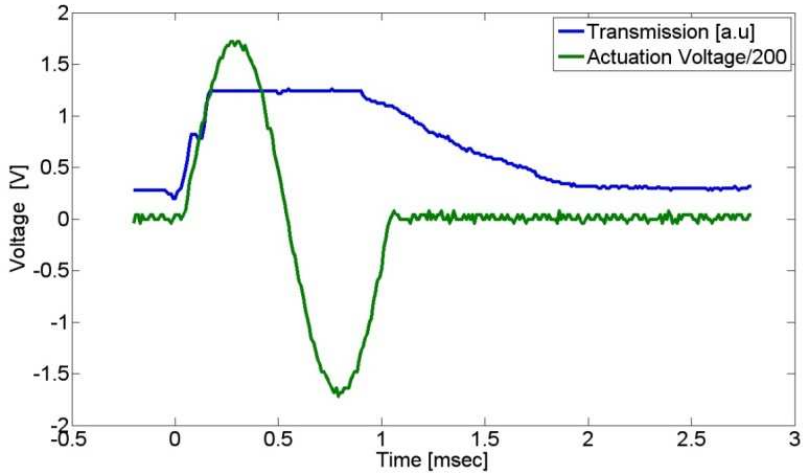

Fig. 7. Time response of the tunable MRR. A single sinusoidal period of the actuation voltage (green) is shown together with the recorded optical transmission in arbitrary voltage units (blue).

Figure 8 is a single frame excerpt from a video of a droplet actuated near the coupling region of the MRR at 10 Hz with 10 periods of 1 kHz sinusoidal voltage in each "on" pulse.

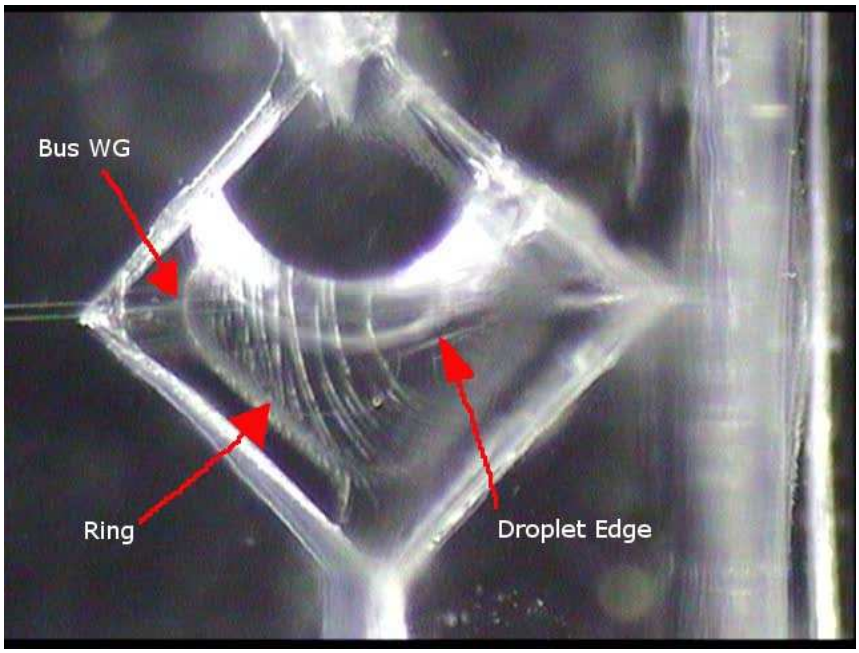

Fig. 8. Single frame excerpt from a video of a droplet actuated near the coupling region of the MRR at 10 Hz (Media 3).

#104407 - $15.00 USD Received 21 Nov 2008; revised 22 Dec 2008; accepted 22 Dec 2008; published 15 Jan 2009

4. Conclusion

The tuning of an on chip MRR via EWOD was demonstrated. Applying voltage to the droplet results in a 0.5 nm redshift in transmission spectrum, which is translated to a modulation depth of up to 31 dB at a fixed wavelength. Response times demonstrated are in the sub-millisecond regime, with rise time of 200 microseconds and fall time of 700 microseconds. The demonstrated device can be used as a tunable notch filter in optical communication applications. Future directions includes miniaturization by using higher index WG material (e.g. silicon), decreasing response times by using smaller droplets, and providing separate control over various optical parameters such as accumulated phase, loss, and coupling strength.

The described approach can be used for the realization of a variety of on chip tunable optical devices actuated by EWOD, with the advantages of high effective refractive index contrast that allows substantial optical modulation, low power consumption and no heating. EWOD actuated tunable optical devices may also be integrated with lab-on-a-chip platform for supporting biosensing and monitoring applications or for more complex and precise optical tuning using multiple miniature droplets.

Acknowledgments

The authors acknowledge the support of the Israeli Science Foundation, the Israeli Ministry of Science, Culture and Sport and the Peter Brojde Center for Innovative Engineering and Computer Science.

#104407 - $15.00 USD Received 21 Nov 2008; revised 22 Dec 2008; accepted 22 Dec 2008; published 15 Jan 2009